Polymerization-Induced Phase Separation: A Maximum in the Intensity of Scattered Light Associated with a Nucleation-Growth Mechanism

Guillermo E. Eliçabe,*,† Hilda A. Larrondo,‡ and Roberto J. J. Williams†

Institute of Materials Science and Technology (INTEMA, University of Mar del Plata, and National Research Council, CONICET) and Department of Physics, Faculty of Engineering, University of Mar del Plata, J. B. Justo 4302, 7600 Mar del Plata, Argentina

Received May 28, 1997; Revised Manuscript Received August 12, 1997[⊗]

ABSTRACT: The appearance of a maximum in the intensity of scattered light at a nonzero wave vector for systems undergoing a polymerization-induced phase separation (PIPS) has been considered in the past as conclusive evidence of the presence of a spinodal demixing mechanism. However, recent results from light scattering studies of colloidal aggregation and phase separation in aqueous biopolymers systems and polymer blends prove that the maximum may also be generated by a nucleation-growth process (NG). The origin of this scattering behavior is the presence of a layer surrounding dispersed-phase particles that contains less solute concentration than the bulk (depletion layer). We apply this concept to a system undergoing PIPS through an NG mechanism. The analysis is constrained to the generation of a diluted dispersion of spherical particles where concentration profiles around particles may be analytically derived. Both Rayleigh−Gans and Mie scattering theories are used to describe the patterns of scattered light. It is shown that in a diffusion-controlled growth process a maximum will appear in the scattered light pattern at a nonzero wave vector. This maximum increases in intensity and shifts to lower values of the wave vector as the population of particles grows. For particular cases where the continuation of nucleation leads to a decrease in the average size of the particles, the maximum may shift to higher values of the wave vector, as recent experimental evidence has demonstrated. For the diluted dispersion, situations where the usual patterns ascribed to NG are obtained, i.e., scattered intensity decaying from the zero wave vector, are (a) the absence of diffusion control in the growth process, (b) starting solutions that are very diluted in the component that will be phase separated, and (c) generation of a very broad distribution of particle sizes.

1. Introduction

Polymerization-induced phase separation (PIPS) is a process by which an initially homogeneous solution of a modifier (rubber, thermoplastic polymer, liquid crystal, etc.) in a mixture of monomers becomes phase separated in the course of reaction. PIPS is used to obtain rubber-modified thermosets, thermoset−thermoplastic blends, polymer-dispersed liquid crystals, etc. Two reviews of this field have been recently published.[1,2]

Phase separation in the pregel state is the result of the change in two different contributions to the free energy of mixing: (a) a decrease in the entropic contribution due to the increase in the oligomer size and (b) a change in the interaction parameter with conversion.[3,4] In the postgel stage an elastic energy contribution has to be included in the analysis.[5] A convenient way to represent the evolution of the system is through a conversion vs composition transformation diagram at constant temperature, generated from free energy vs composition curves at different conversions.[2−9] Figure 1 shows such a diagram. The dashed line represents a formulation that enters the metastable region at a particular conversion in the polymerization reaction. Point A represents a metastable condition, whereas points B and C are the corresponding equilibrium concentrations.

Phase separation in the metastable region may proceed through a nucleation-growth (NG) mechanism. The possibility that this mechanism takes place depends on

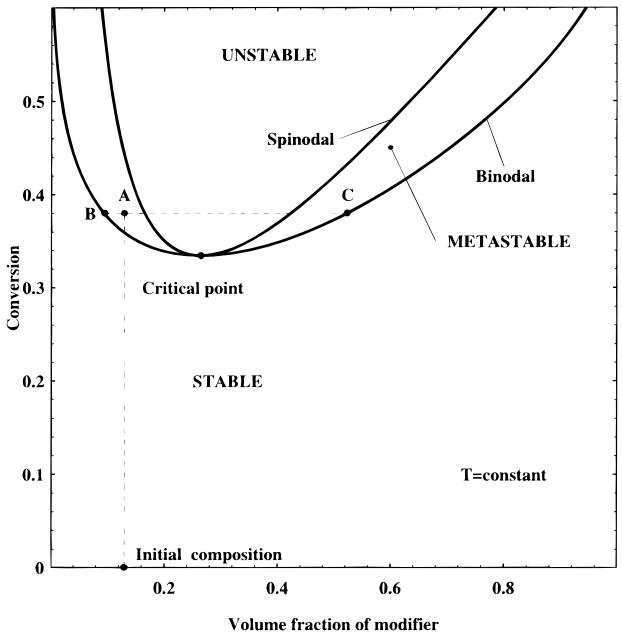

Figure 1. Binodal and spinodal curves in a conversion vs composition transformation diagram at constant temperature. The critical point and the locations of stable, metastable, and unstable regions are shown.

the relative rates of phase separation and polymerization:

$$K = \text{phase separation rate/polymerization rate}$$

If $K \rightarrow \infty$, equilibrium is instantaneously reached and the system evolves along both branches of the binodal

†INTEMA.
‡Department of Physics.
⊗ Abstract published in *Advance ACS Abstracts,* October 1, 1997.

S0024-9297(97)00754-7 CCC: $14.00

curve. If $K \rightarrow 0$, no phase separation will be observed until the spinodal curve is reached and spinodal demixing (SD) takes place. Actual K values lead to trajectories that may be fully located in the metastable region, in which case phase separation takes place exclusively by an NG mechanism, or that may enter the unstable region, implying that SD has to be considered to account for the morphologies generated. However, according to Inoue,[1,10−13] the NG mechanism cannot take place at all because homogeneous nucleation is an extremely slow process. The appearance of a maximum in the scattered light intensity at a nonzero wave vector is consistently considered as conclusive evidence of the presence of SD.[1,14] Several authors have interpreted their experimental results in this direction,[15,16] while other authors insist on the possible presence of an NG mechanism to account for the observed experimental trends.[7,17−27] For a particular system described by an NG mechanism, a peak in the scattered intensity at a nonzero wave vector was observed.[28]

In this context, it must be accepted that either the picture of phase separation occurring entirely through NG is incorrect or the consideration of the presence of a maximum in the scattered light as the hallmark of spinodal demixing may be questioned.

A possible answer to this controversy arises from colloidal aggregation studies using light scattering[29,30] which are based on results of previous publications dealing with the growth of semiconductor nanocrystals in a glassy matrix.[31] In these studies it was found that the scattering intensity profile $I(q)$, with q being the magnitude of the scattering wave vector, $q = (4\pi/\lambda)\sin(\theta/2)$, λ the wavelength of the incident light in vacuum, and θ the scattering angle, exhibited a peak value I_m at a nonzero wave vector q_m, with I_m increasing and q_m decreasing in the course of the growing process. A scaling behavior of $I(q)$, somewhat similar to that observed in SD, was evidenced. The physical origin of the peak of $I(q)$ lies in the fact that the aggregates grow by depleting a region surrounding the aggregate. Mass conservation applied to the volume enclosing the cluster/crystal plus its depletion region leads to $I(0) = 0$ and, consequently, to the presence of a peak in $I(q)$ as was theoretically modeled.[30] The presence of the peak does not imply any ordering in the spatial arrangement of clusters/crystals.

Very recently, Tromp and Jones[32] reported experimental results for the off-critical phase separation and gelation in solutions of gelatin and dextran. Phase separation leading to a distribution of isolated dextran-rich spheres in a gelatin-rich matrix was followed with small-angle light scattering. A maximum in the light-scattering pattern was observed, which was modeled following Carpineti et al.,[30] i.e., the scattering of a dense nucleus surrounded by a dilute depletion layer.

In another recent paper, Balsara et al.[33] studied the early stages of nucleation and growth in a polymer blend located in the metastable region of the phase diagram by time-resolved neutron scattering (SANS). At intermediate stages of the phase separation, a scattering maximum developed and the intensity increased rapidly with time. One possible explanation of this maximum was the formation of a depletion zone around the growing clusters.[34]

We will show that the presence of a depletion layer surrounding growing particles may explain the presence of a maximum in the pattern of scattered light obtained during PIPS. The shift of the peak's intensity and angular position during the evolution of the population of dispersed-phase particles will be discussed. However, the analysis will be restricted to the case of a diluted dispersion, i.e., a situation in which depletion layers do not get in contact. Work is in progress to extend the analysis to concentrated dispersions. Preliminary results indicate that it is possible to generate a maximum in the pattern of scattered light without the need to rely on the existence of depletion layers. This will be the object of a next publication.

2. Theory

2.1. Depletion Layer. Let us consider the system placed at point A (Figure 1), inside the metastable region. At these conditions, nucleation is taking place, leading to particles of radii R_c (critical radius). In fact, the size of these nuclei may be on the order of the largest species of the modifier distribution (e.g., a rubber), as arises from simulations using a phase separation model.[6,7,25] Nucleation may be thus considered as a heterogeneous event, as suggested by Binder.[35] The modifier (e.g., a rubber) concentration inside the particle is $\rho_A^{(n)}$, expressed in terms of mass of A per unit volume and read at point C in Figure 1 (in fact, the concentration that minimizes the free energy is located somewhat to the right of point C,[6,7] but we will neglect this small shift in the present analysis). The modifier concentration at the interface is the equilibrium concentration, $\rho_A^{(eq)}$, read at point B in Figure 1.

The $\rho_A(r,t)$ profile in the region surrounding a particle of constant radius R_n may be obtained by solving the differential mass balance written with constant values of the overall density (ρ) and the diffusion coefficient (D). The general problem to be solved is that of a moving boundary in a medium where composition varies with both position and time.

A limiting case of the problem is to consider a pseudo-steady-state in the layer surrounding the particle ($t \gg R_n^2/\pi D$). This hypothesis is frequently stated in the analysis of growth laws[36] and may be shown to be valid for particles with sizes comprised in the range of nanometers to microns and time scales typical of the PIPS. Under this condition, the mass balance reads

$$\mathrm{d}/\mathrm{d}r\,(r^2\,\mathrm{d}\rho_A/\mathrm{d}r) = 0 \qquad (1)$$

with $\rho_A = \rho_A^{(eq)}$ at $r = R_n$ and $\rho_A = \rho_A^{(0)}$ for $r \rightarrow \infty$. In order to avoid the asymptotic convergence to the initial concentration, the solution will be truncated assuming that $\rho_A = \rho_A^{(0)}$ at $r = R_d$ and setting the R_d value through a mass balance. This leads to

$$[\rho_A^{(0)} - \rho_A]/[\rho_A^{(0)} - \rho_A^{(eq)}] = (1/r - 1/R_d)/(1/R_n - 1/R_d) \qquad (2)$$

This is the same concentration profile proposed by Tromp and Jones,[32] on an empirical basis, to fit their experimental $I(q)$ vs q curves.

Therefore, the diffusion-controlled growth of particles predicts the generation of a depletion layer of thickness $R_d - R_n$, where the modifier concentration decreases from the bulk value $\rho_A^{(0)}$ to $\rho_A^{(eq)}$. The R_d value may be obtained from eq 2 and the mass conservation principle:

$$[\rho_A^{(0)} - \rho_A^{(eq)}]/[\rho_A^{(n)} - \rho_A^{(0)}] = 2(1 - R_n/R_d)/[(R_d/R_n)^2 + 2(R_n/R_d) - 3] \qquad (3)$$

As can be visualized from Figure 1, usually $[\rho_A^{(0)} - \rho_A^{(eq)}]$ (segment AB) is significantly smaller than $[\rho_A^{(n)} - \rho_A^{(0)}]$ (segment AC), particularly for off-critical compositions. Values of R_d/R_n for simulation purposes will be taken in the range $R_d/R_n = 2-10$, implying that AB/AC varies from 0.5 to 0.0185. Solutions that are very diluted in the modifier, i.e., low values of $\rho_A^{(0)}$, will lead to large R_d/R_n ratios due to the necessity of increasing the radius R_d to fulfill the mass balance.

Equations 2 and 3 are also valid for a diluted dispersion, such that the initial composition, $\rho_A^{(0)}$, still persists outside the depletion layer of every individual sphere. The model is valid up to a particular volume fraction of the dispersed phase, φ, limited by $\varphi^{max} = (R_n/R_d)^3$.

2.2. Light Scattering Pattern of the Growing Particles. The proposed model gives rise to an ensemble of scatterers that consists of coated spherical particles which are randomly located. The coat of these coated particles is the depletion layer. The theory of light scattering by spherical particles is well-known and can be found in textbooks.[37-39] Here we will only give a brief account of what is relevant for this work.

As we are considering a diluted dispersion, the particles in the ensemble behave as independent scatterers; i.e., there is no systematic relation between the phases of the waves scattered by different particles. Then, only the light scattered by one particle needs to be considered. The total light scattered by the ensemble will be just the sum of the light intensities scattered by each one of the individual particles.

When the difference in refractive indices between the particles and the surrounding medium is small and the particles are not too large, Rayleigh−Gans (RG) scattering can be successfully used to describe the light-scattering pattern, $I(q)$, of ensembles of spherical particles. Indeed, this is normally done when light patterns of phase-separating systems are modeled.[32]

RG scattering leads to analytical expressions for the intensity of light dispersed by one spherical particle. This intensity $i(q)$, corrected by the polarization factor, $I(q) = i(q)\, 2/(1 + \cos^2\theta)$, for incident unpolarized light, is given by:

$$I(q) \sim \left[\frac{4\pi}{q}\int_0^{R_d} \Delta n(r)\, r \sin(rq)\, dr\right]^2 \qquad (4)$$

where $\Delta n(r) = n(r) - n_0$ is the relative refractive index profile inside the particle and R_d is the radius of the particle (considered as the core plus the depletion layer).

When the difference in refractive index is not small or the particles are large compared with the wavelength of the incident light, instead of eq 4 the full solution of the Maxwell equations for a single particle must be considered. This solution is known as the Mie theory. Analytical solutions using this theory for particles of different regular geometries are available in the literature. In particular, the solutions for homogeneous spherical particles and coated spherical particles can be found in Bohren and Huffman.[37] Unfortunately, the coated spherical particles in our problem have variable refractive indices along the coat, and to our knowledge, there is no closed solution for this problem in the literature.

Under the Mie regime the pattern of scattered light can be obtained from

$$I(q) \sim \int_0^{\infty} S_{11}(q,R_d)\, f(R_d)\, dR_d \qquad (5)$$

for incident unpolarized light. Here, S_{11} is the (1,1) element of the scattering matrix of a coated sphere of outer radius R_d,[37] and $f(R_d)$ is the number distribution of outer radii of the particles in the sample. The effect of polydispersity introduced by $f(R_d)$ in eq 5 can be easily incorporated into eq 4 of the RG approximation. In all our calculations the ratio of the outer radius to the inner radius R_n in a given sample was taken to be the same for all particles.

In principle, RG and Mie scattering are suitable candidate models to compute the light patterns of the growing particles. With RG it is possible to impose a profile of a refractive index for the depletion layer, such as the one calculated in the previous section. Under the Mie regime all sizes and refractive indices can be considered, but the coat is constrained to have a constant refractive index.

3. Results and Discussion

3.1. Model Selection. In order to select a light-scattering model for this study we have calculated $I(q)$ for different cases. This initial test was conducted using typical values of particle size and depletion layer thickness.

Refractive indices were assigned for this test and for the rest of the calculations as follows. For the continuous phase with concentration $\rho_A^{(0)}$, $n_0 = 1.6$ (a typical value of some epoxyamine matrices[40]). For the dispersed phase with concentration $\rho_A^{(n)}$, $n_n = 1.5$ (a typical value of some rubber modifiers[41]). For the depletion layer, the refractive index is taken as a linear function of composition:

$$n_d(\rho_A) = 1.6 + 0.1[\rho_A^{(0)} - \rho_A]/[\rho_A^{(n)} - \rho_A^{(0)}] \qquad (6)$$

where ρ_A varies from $\rho_A^{(0)}$ to $\rho_A^{(eq)}$.

By substituting eqs 2 and 3 in eq 6, n_d may be written as

$$n_d(r) = 1.60 + 0.2[R_n/r - R_n/R_d]/[(R_d/R_n)^2 + 2(R_n/R_d) - 3] \qquad (7)$$

Equation 7 gives the n_d profile to be used in the RG approximation.

On the other hand, to employ the Mie scattering theory, an average concentration in the depletion layer will be assumed in order to have a homogeneous coat. This is given by

$$\rho_A^{(av)} = \int_{R_n}^{R_d} \rho_A(r)\, r^2\, dr / \int_{R_n}^{R_d} r^2\, dr \qquad (8)$$

Substituting eq 2 into eq 8, solving, and using eq 3, we obtain

$$[\rho_A^{(0)} - \rho_A^{(av)}]/[\rho_A^{(n)} - \rho_A^{(0)}] = 1/[(R_d/R_n)^3 - 1] \qquad (9)$$

The average refractive index of the depletion layer is obtained by substituting eq 9 into eq 6 to give

$$n_d^{(av)} = 1.6 + 0.1/[(R_d/R_n)^3 - 1] \qquad (10)$$

Thus, $n_d^{(av)}$ varies from 1.6143 for $R_d/R_n = 2$ to 1.6001 for $R_d/R_n = 10$.

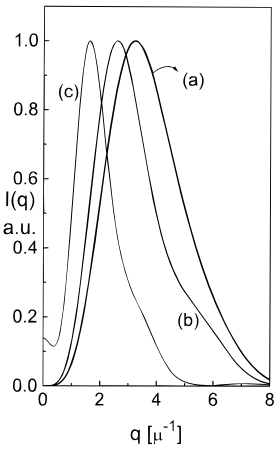

Figure 2. Normalized light-scattering intensity spectra of monodisperse particles of $R_n = 500$ nm and $R_d/R_n = 4$, predicted by three different models: (a) RG with $n_d(r)$, (b) RG with $n_d^{(av)}$, (c) Mie with $n_d^{(av)}$.

The initial test was conducted for a sample of monodisperse particles with $R_n = 500$ nm and $R_d = 2000$ nm ($R_d/R_n = 4$). Equations 7 and 10 for $R_d/R_n = 4$ give the values of refractive index of the depletion layer to be used; i.e., $n_d(r) = 1.596 + 7.407/r$ for the RG theory and $n_d^{(av)} = 1.6016$ for the Mie theory (eq 5).

In Figure 2 light patterns are calculated for three different cases: RG scattering with $n_d(r)$ (eq 4), RG scattering with $n_d^{(av)}$ (eq 4), and Mie scattering with $n_d^{(av)}$ (eq 5). The light profiles thus obtained are similar to each other. Apart from the different positions of the maxima, the only strong difference is between the RG profiles and the Mie profile. The former vanish at zero angle, whereas the latter has its first local maximum at zero. This feature makes this profile qualitatively different from those calculated using RG; i.e., linear combinations of RG profiles will always vanish at zero angle; however, linear combinations of Mie profiles may even take the maximum in intensity to disappear. As we are considering the conditions under which a maximum at a nonzero wave vector appears in the light-scattering pattern, the Mie model is better suited than the RG approximation; i.e., when the mass balance associated with the depletion layer is replaced in the RG model, the intensity will always be zero at $q = 0$, meaning that a maximum at a nonzero wave vector will be present. From now on, the results presented are based on the assumption that scattering obeys Mie theory for a homogeneous particle surrounded by a homogeneous coat.

3.2. Influence of Model Parameters. Figure 3a shows the size distributions assumed for the outer radii of the growing particles, for different values of R_d/R_n. These distributions are Gaussian with a mean radius of the growing core, $\bar{R}_n = 125$ nm, and a standard deviation of 35 nm. The ratio R_d/R_n was taken as 2, 4, 6, 8, and 10. In Figure 3b the light-scattering patterns of particles with radii as the mean radii of the distributions in Figure 3a are shown. The light-scattering profiles corresponding to the size distributions of Figure 3a are displayed in Figure 3c. For the same number of particles, as R_d/R_n is increased, the peak in the scattering spectrum is shifted to the left and the intensity increases. The spectra of the polydisperse particles are shifted to the left with respect to those of the monodisperse ones. This can be anticipated because the larger particles in the distribution, whose maxima occur at

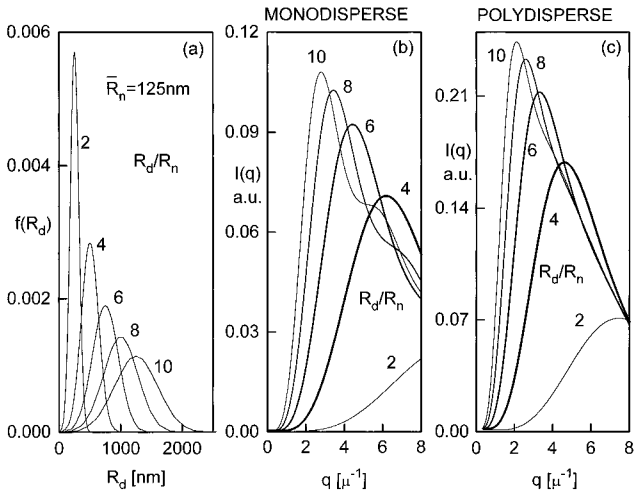

Figure 3. (a) Size distribution of outer radii of growing particles ($\bar{R}_n = 125$ nm, $\sigma = 35$ nm), for different values of R_d/R_n. (b) Light-scattering intensity spectra of monodisperse particles of the same radius as the mean radius of distribution in part a, for different values of R_d/R_n. (c) Light-scattering intensity spectra of polydisperse particles, with radius distributions as in part a, for different values of R_d/R_n.

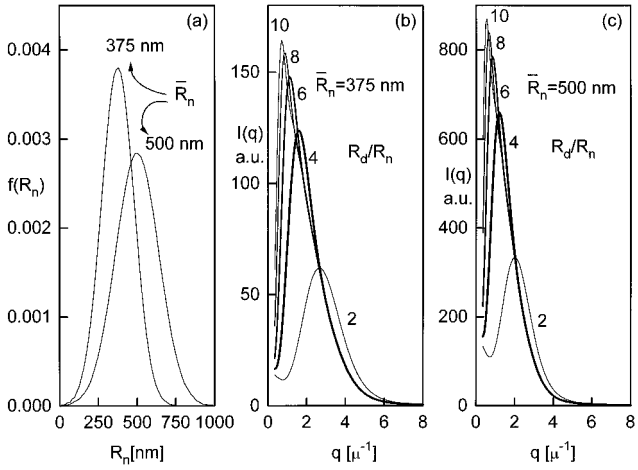

Figure 4. (a) Size distribution of inner radii of growing particles: $\bar{R}_n = 375$ nm ($\sigma = 105$ nm) and $\bar{R}_n = 500$ nm ($\sigma = 140$ nm). (b) Light-scattering intensity spectra of polydisperse particles with depletion layers, with radius distribution as in part a ($\bar{R}_n = 375$ nm), for different values of R_d/R_n. (c) Light-scattering intensity spectra of polydisperse particles with depletion layers, with radius distribution as in part a ($\bar{R}_n = 500$ nm), for different values of R_d/R_n.

smaller values of q, scatter more strongly than the smaller particles.

In Figure 4 the light-scattering patterns obtained using distributions with mean radii of 375 (standard deviation 105 nm) and 500 nm (standard deviation 140 nm) are displayed. These results confirm the tendencies observed in the example of Figure 3.

In all the examples above, a maximum in intensity at a nonzero wave vector is observed. Its position in the light pattern is essentially determined by the ratio of outer to inner radii. As this ratio increases, the peak moves to the left. This displacement may take the peak out of the observation range of the instrument. This will be the case for formulations very diluted in the modifier that originate large R_d/R_n ratios to fulfill the mass balance (eq 3). However, this is not the only instance in which the peak is not going to arise. In Figure 5 log-normal distributions of growing particles are used to generate light-scattering profiles. The

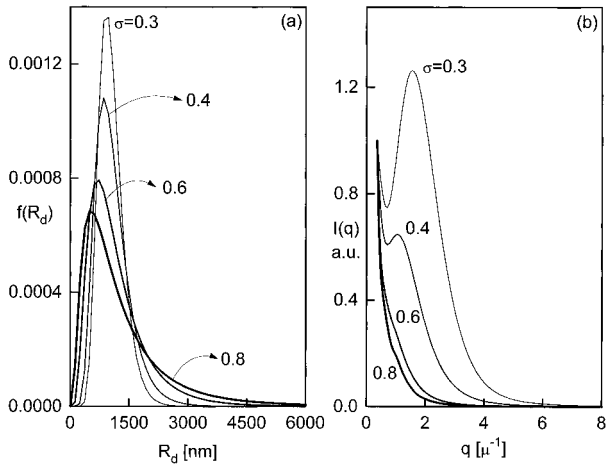

Figure 5. (a) Lognormal size distribution of outer radii of growing particles: $\bar{R}_n = 500$ nm, $R_d/R_n = 2$, and $\sigma = 0.3$, 0.4, 0.6, and 0.8. (b) Normalized light-scattering intensity spectra of polydisperse particles with depletion layers, with radius distributions as in part a.

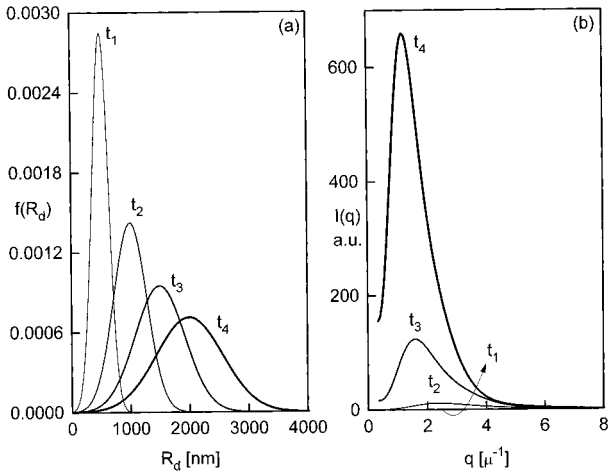

Figure 6. (a) Size distributions of outer radii of growing particles: $\bar{R}_d = 500$ nm and $\sigma = 140$ nm (t_1); $\bar{R}_d = 1000$ nm and $\sigma = 280$ nm (t_2); $\bar{R}_d = 1500$ nm and $\sigma = 420$ nm (t_3); $\bar{R}_d = 2000$ nm and $\sigma = 560$ nm (t_4), $R_d/R_n = 4$. (b) Light-scattering profiles of the distributions in part a.

distributions are all of 500 nm of mean radius, with standard deviations (as defined in a log-normal distribution) of 0.3, 0.4, 0.6, and 0.8 nm. The light-scattering profile for the more narrow distribution shows clearly a maximum at a nonzero q. As the standard deviation is increased and the distribution broadened, the maximum tends to shift to the left and to get blurred. For a certain breadth of the distribution the peak disappears. It is worth noting that this result can only be arrived at if Mie scattering is considered. In the RG approximation the light profiles decay to zero at zero q in all cases, and then any linear combination of them, which is the basic operation needed to compute the polydisperse cases, will also vanish at zero angle, giving rise to the maximum in intensity at nonzero q.

3.3. Shift in Light Scattering Patterns during PIPS. Now we will make the first reference to time by postulating some hypothetical evolution of the distribution of the population of growing particles. Figure 6a represents a narrow distribution of small particles evolving in time by increasing its mean radius (125, 250, 375, and 500 nm) and its standard deviation (35, 70, 105, and 140 nm) while keeping depletion layers around the cores. In this very simplified picture of the growing

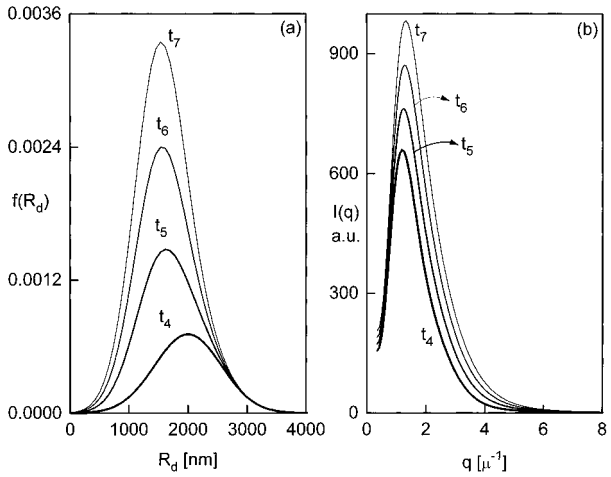

Figure 7. (a) Size distributions of outer radii of growing particles: $\bar{R}_d = 2000$ nm and $\sigma = 560$ nm (t_4); $\bar{R}_d = 1750$ nm and $\sigma = 554$ nm (t_5); $\bar{R}_d = 1667$ nm and $\sigma = 526$ nm (t_6); $\bar{R}_d = 1625$ nm and $\sigma = 507$ nm (t_7), $R_d/R_n = 4$. (b) Light-scattering profiles of the distributions in part a.

process we have assumed that the number of particles remains the same along time. A fixed value of $R_d/R_n = 4$ was assumed at every time instant. In Figure 6b the light-scattering patterns corresponding to the distributions at times t_1, t_2, t_3, and t_4 are displayed. The spectrum at time t_1 cannot be distinguished at the scale of the figure. The spectra for the larger times evolve by increasing I_m and shifting q_m to the left with time. This evolution could be easily ascribed to a system undergoing SD, although it was generated by a random dispersion of growing particles.

Another possible situation is depicted in Figure 7. Here the results for a particular hypothetical evolution of the system beyond t_4 are shown. In this period from t_4 to t_7, the continuation of the nucleation process makes the distribution of sizes decrease its mean value and broaden.[25,42] The number of particles is now increased from t_4 on. At time t_5 the number of particles is doubled with respect to t_4, at time t_6 it is tripled, and at time t_7 it is quadrupled. The light-scattering spectra are shown in Figure 7b where it can be noticed that the evolution is such that I_m increases with time and q_m shifts to the right as time goes on. Experimental results showing this trend have been recently reported.[16]

4. Conclusions

Recent results from light-scattering studies of colloidal aggregation,[29,30] phase-separation processes in aqueous biopolymer systems,[32] and polymer blends[33] have been brought forward to give a possible answer to a controversy on the mechanism of polymerization-induced phase separation in a variety of systems.

The light-scattering patterns of a dilute dispersion of randomly located growing particles with depletion layers have been investigated through simulations using the results of Mie scattering theory for a homogeneous core surrounded by a homogeneous coat. The results show that, in many situations, a maximum in the intensity of scattered light may be observed. This maximum, which has been considered in the past as the hallmark of SD, may arise also in a system where phase separation occurs by an NG mechanism.

During PIPS there is a continuous evolution in the size and number distribution of the population of dispersed-phase particles. For the usual case where the average size and the standard deviation increase, the

I_m shifts to lower q values (a case frequently observed and reported as arising from an SD mechanism). But, for cases where nucleation prevails over growth, i.e., late stages of phase separation in a high-viscosity medium, the number of particles may increase with a corresponding decrease in the average size. This produces a shift of I_m to higher q values (a case recently reported and ascribed to nucleation-induced spinodal demixing[16]).

For a diluted dispersion of spheres, NG will not lead to a maximum in the scattered light at a nonzero wave vector when (a) particle growth is not controlled by diffusion, i.e., depletion layers are not produced; (b) the starting solution is highly diluted, leading to large R_d/R_n ratios; and (c) very broad distributions of particle sizes are generated.

References and Notes

(1) Inoue, T. *Prog. Polym. Sci.* **1995**, *20*, 119.
(2) Williams, R. J. J.; Rozenberg, B. A.; Pascault, J. P. *Adv. Polym. Sci.* **1997**, *128*, 95.
(3) Borrajo, J.; Riccardi, C. C.; Williams, R. J. J.; Cao, Z. Q.; Pascault, J. P. *Polymer* **1995**, *36*, 3541.
(4) Riccardi, C. C.; Borrajo, J.; Williams, R. J. J.; Girard-Reydet, E.; Sautereau, H.; Pascault, J. P. *J. Polym. Sci., B: Polym. Phys.* **1996**, *34*, 349.
(5) Borrajo, J.; Riccardi, C. C.; Williams, R. J. J.; Masood Siddiqi, H.; Dumon, M.; Pascault, J. P. *Polymer* **1997**, in press.
(6) Williams, R. J. J.; Borrajo, J.; Adabbo, H. E.; Rojas, A. J. In *Rubber-Modified Thermoset Resins*; Riew, C. K., Gillham, J. K., Eds.; Advances in Chemistry Series 208; American Chemical Society: Washington, DC, 1984; p 195.
(7) Vazquez, A.; Rojas, A. J.; Adabbo, H. E.; Borrajo, J.; Williams, R. J. J. *Polymer* **1987**, *28*, 1156.
(8) Riccardi, C. C.; Borrajo, J.; Williams, R. J. J. *Polymer* **1994**, *35*, 5541.
(9) Clarke, N.; McLeish, T. C. B.; Jenkins, S. D. *Macromolecules* **1995**, *28*, 4650.
(10) Yamanaka, K.; Inoue, T. *Polymer* **1989**, *30*, 662.
(11) Yamanaka, K.; Takagi, Y.; Inoue, T. *Polymer* **1989**, *30*, 1839.
(12) Yamanaka, K.; Inoue, T. *J. Mater. Sci.* **1990**, *25*, 241.
(13) Ohnaga, T.; Chen, W.; Inoue, T. *Polymer* **1994**, *35*, 17.
(14) Hashimoto, T. In *Current Topics in Polymer Science*; Ottenbrite, R. M., Utracki, L. A., Inoue, S., Eds.; Hanser Publishers: Munich, 1987; Vol. II, p 199.
(15) Kim, D. S.; Kim, S. Ch. *Polym. Eng. Sci.* **1994**, *34*, 1598.
(16) Kyu, Th.; Lee, J. H. *Phys. Rev. Lett.* **1996**, *76*, 3746.
(17) Ruseckaite, R. A.; Williams, R. J. J. *Polym. Int.* **1993**, *30*, 11.
(18) Ruseckaite, R. A.; Hu, L.; Riccardi, C. C.; Williams, R. J. J. *Polym. Int.* **1993**, *30*, 287.
(19) Ruseckaite, R. A.; Fasce, D. P.; Williams, R. J. J. *Polym. Int.* **1993**, *30*, 297.
(20) Chen, J. P.; Lee, Y. D. *Polymer* **1995**, *36*, 55.
(21) Kim, S. Ch.; Ko, M. B.; Jo, W. H. *Polymer* **1995**, *36*, 2189.
(22) Verchere, D.; Sautereau, H.; Pascault, J. P.; Riccardi, C. C.; Moschiar, S. M.; Williams, R. J. J. *Macromolecules* **1990**, *23*, 725.
(23) Verchere, D.; Sautereau, H.; Pascault, J. P.; Moschiar, S. M.; Riccardi, C. C.; Williams, R. J. J. *J. Appl. Polym. Sci.* **1990**, *41*, 467.
(24) Verchere, D.; Pascault, J. P.; Sautereau, H.; Moschiar, S. M.; Riccardi, C. C.; Williams, R. J. J. *J. Appl. Polym. Sci.* **1991**, *42*, 701.
(25) Moschiar, S. M.; Riccardi, C. C.; Williams, R. J. J.; Verchere, D.; Sautereau, H.; Pascault, J. P. *J. Appl. Polym. Sci.* **1991**, *42*, 717.
(26) Verchere, D.; Pascault, J. P.; Sautereau, H.; Moschiar, S. M.; Riccardi, C. C.; Williams, R. J. J. *J. Appl. Polym. Sci.* **1991**, *43*, 293.
(27) Verchere, D.; Sautereau, H.; Pascault, J. P.; Moschiar, S. M.; Riccardi, C. C.; Williams, R. J. J. In *Toughened Plastics I: Science and Engineering*; Riew, C. K., Kinloch, A. J., Eds.; Advances in Chemistry Series 233; American Chemical Society: Washington, DC, 1993; p 335.
(28) Chen, D.; Pascault, J. P.; Sautereau, H.; Vigier, G. *Polym. Int.* **1993**, *32*, 369.
(29) Carpineti, M.; Giglio, M. *Phys. Rev. Lett.* **1992**, *68*, 3327.
(30) Carpineti, M.; Giglio, M.; Degiorgio, V. *Phys. Rev. E* **1995**, *51*, 590.
(31) Banfi, G. P.; Degiorgio, V.; Rennie, A.; Barker, J. *Phys. Rev. Lett.* **1992**, *69*, 3401.
(32) Tromp, R. H.; Jones, R. A. L. *Macromolecules* **1996**, *29*, 8109.
(33) Balsara, N. P.; Lin, Ch.; Hammouda, B. *Phys. Rev. Lett.* **1996**, *77*, 3847.
(34) Schatzel, K.; Ackerson, B. J. *Phys. Rev. E* **1993**, *48*, 3776.
(35) Binder, K. *J. Chem. Phys.* **1983**, *79*, 6387.
(36) Marqusee, J. A.; Ross, J. *J. Chem. Phys.* **1984**, *80*, 536.
(37) Bohren, C. F.; Huffman, D. R. *Absorption and Scattering of Light by Small Particles;* John Wiley & Sons: New York, 1983.
(38) van de Hulst, H. C. *Light Scattering by Small Particles*; John Wiley & Sons: New York, 1957.
(39) Jackson, J. D. *Classical Electrodynamics*; John Wiley & Sons: New York, 1975.
(40) Kim, B. S.; Chiba, T.; Inoue, T. *Polymer* **1995**, *36*, 67.
(41) Brandrup, J.; Immergut, E. H. *Polymer Handbook*, 2nd ed.; John Wiley & Sons: New York, 1975.
(42) Nikitin, O. V.; Rozenberg, B. A. *Polym. Sci. USSR* **1992**, *34*, 365.

MA9707547